JGR Oceans

RESEARCH ARTICLE
10.1029/2019JC015500

On the Differences Between the South Pacific Meridional and Quadrupole Modes

Ruiqiang Ding[1,2], Jianping Li[2], Ruowen Yang[3], Yu-heng Tseng[4], Yang Li[5], and Kai Ji[6]

[1]State Key Laboratory of Earth Surface Processes and Resource Ecology, Beijing Normal University, Beijing, China, [2]Key Laboratory of Physical Oceanography-Institute for Advanced Ocean Studies, Ocean University of China and Qingdao National Laboratory for Marine Science and Technology, Qingdao, China, [3]Department of Atmospheric Sciences, Yunnan University, Kunming, China, [4]Institute of Oceanography, National Taiwan University, Taipei, Taiwan, [5]Plateau Atmosphere and Environment Key Laboratory of Sichuan Province, Chengdu University of Information Technology, Chengdu, China, [6]College of Atmospheric Sciences, Lanzhou University, Lanzhou, China

Key Points:
- The SPQ and SPMM are different in terms of their spatial structure, temporal variations, and impacts on ENSO
- In contrast to the SPMM, the SPQ includes an additional component of SSTAs in the southwest Pacific and high-latitude South Pacific
- The SPQ is more closely linked than the SPMM to ENSO, and the SPQ may represent a more reliable precursor than the SPMM for ENSO events

Supporting Information:
- Supporting Information S1

Correspondence to:
R. Ding,
drq@mail.iap.ac.cn

Citation:
Ding, R., Li, J., Yang, R., Tseng, Y.-h., Li, Y., & Ji, K. (2020). On the differences between the South Pacific meridional and quadrupole modes. *Journal of Geophysical Research: Oceans*, *125*, e2019JC015500. https://doi.org/10.1029/2019JC015500

Received 18 JUL 2019
Accepted 20 DEC 2019
Accepted article online 6 JAN 2020

Abstract The South Pacific quadrupole (SPQ) and South Pacific meridional mode (SPMM) are the dominant modes of South Pacific sea surface temperature (SST) variability. Both SST modes have been found to affect the occurrence of El Niño-Southern Oscillation (ENSO) events. In this study, the authors examine the differences between the SPQ and SPMM in terms of their spatial structure, temporal variations, and impacts on ENSO using observational and Coupled Model Intercomparison Project Phase 5 (CMIP5) model data. As a local SST mode defined in the subtropical southeast Pacific, the SPMM has large-amplitude SST anomalies (SSTAs) mainly confined in the southeast Pacific. In contrast, as a basin-scale SST mode defined in the South Pacific basin, the SPQ has large-amplitude SSTAs over the southeast Pacific as well as over the southwest Pacific and high-latitude South Pacific. In addition, the SPQ has its temporal variability independent of the SPMM, and the occurrence of strong SPQ events is not always simultaneous with strong SPMM events. The SPQ is more closely linked than the SPMM to ENSO, possibly because the SPQ includes an additional component of SSTAs in the southwest Pacific and high-latitude South Pacific. These findings suggest that compared with the SPMM, the SPQ may act as an improved precursor signal for ENSO events. The results have implications for understanding the respective roles of SSTAs over different regions of the South Pacific in influencing ENSO.

Plain Language Summary El Niño-Southern Oscillation (ENSO) is known to have profound impacts on worldwide climate systems, and a better understanding of the effect of the South Pacific sea surface temperature (SST) modes on ENSO may help to improve the skill of climate predictions. In this study, we show that two dominate modes of South Pacific SST variability, the South Pacific quadrupole (SPQ) and South Pacific meridional mode (SPMM), have different impacts on ENSO. The SPQ is more closely linked than the SPMM to ENSO for lead times of up to a year, suggesting that the SPQ may represent a more reliable precursor signal than the SPMM for ENSO events. The reason for this is may be that the SPQ includes an additional component of SST anomalies (SSTAs) in the southwest Pacific and high-latitude South Pacific.

1. Introduction

The North Pacific meridional mode (NPMM) is a leading mode of covariability in sea surface temperature (SST) and surface winds in the northeasterly trade regime (Chiang & Vimont, 2004). It is initiated by the North Pacific Oscillation (Rogers, 1981) by altering the northeasterly trade winds on the southern flank of the North Pacific Oscillation during boreal winter and evolves via positive feedback known as the wind-evaporation-SST (WES) feedback (Xie & Philander, 1994) between the wind-induced evaporation and the underlying SSTs during boreal spring. The atmosphere-ocean coupling then sustains the NPMM-related SST anomalies (SSTAs) from boreal spring to the following summer, which subsequently force anomalous equatorial westerly winds over the western Pacific that may contribute to the development of El Niño-Southern Oscillation (ENSO) events through triggering the Bjerknes feedback (the seasonal footprinting mechanism [SFM]; Vimont et al., 2003, Vimont et al., 2003). Therefore, it has been suggested that the NPMM may act as an ocean conduit through which the extratropical atmosphere influences ENSO (Zhang et al., 2009).

There is a long history of studies of the relationships between North Pacific extratropical atmospheric variability, the NPMM, and ENSO (e.g., Chang et al., 2007; Ding et al., 2015; Larson & Kirtman, 2013; Lin et al., 2015; Zhang et al., 2009). In contrast, ENSO precursors emanating from the South Pacific have received less attention. Recently, the South Pacific meridional mode (SPMM), which is the South Pacific counterpart to the NPMM, has been identified in the subtropical southeast Pacific (Zhang et al., 2014; Zhang et al., 2014). The SPMM bears some resemblance to the NPMM in terms of its physical interpretation. That is, changes in the southeasterly trade winds originating outside the tropical Pacific alter the evaporation and SST and then initiate a positive WES feedback that is vital in the formation of the SPMM. Through the SFM, the SPMM is also shown to be intimately linked to the development of ENSO (Larson et al., 2018; You & Furtato, 2018; Zhang, Clement, & Di Nezio, 2014). While physically analogous to the NPMM, some studies have also suggested that there are some differences between the NPMM and SPMM in terms of their influences on ENSO. For example, Zhang, Clement, and Di Nezio (2014) found that the SPMM has a stronger equatorial expression than the NPMM. Matei et al. (2008) found that the SPMM has a larger and faster impact on the tropical Pacific than the NPMM. Min et al. (2017) reported that the NPMM and SPMM tend to induce the development of SSTAs in the central and eastern equatorial Pacific, respectively. Despite these differences, both the NPMM and SPMM are viewed as potentially important precursors for ENSO events (Min et al., 2017).

In addition to the SPMM in the subtropical southeast Pacific, the extratropical South Pacific Ocean has been suggested to affect the development of ENSO. Ding et al. (2015) reported that a quadrupole SSTA pattern in the extratropical South Pacific, which was labeled the South Pacific quadrupole (SPQ), exerts a forcing effect on ENSO through the SFM. The SPQ shares characteristics with the SPMM, with their related SSTAs overlapping over some regions of the South Pacific. Both the SPQ and SPMM mainly favor the development of SSTAs in the eastern equatorial Pacific (i.e., the eastern Pacific-type ENSO) (Ding, Li, & Tseng, 2015; Min et al., 2017). However, given that the SPMM and SPQ represent a subtropical and extratropical mode of South Pacific climate variability, respectively, it is likely that there are major differences between their influences on ENSO. It is worth investigating the relative roles of the SPQ and SPMM in initiating ENSO and further understanding to what extent the SPQ→ENSO process can occur independently of the SPMM→ENSO process. In this study, we will investigate in detail the differences between the SPQ and SPMM in terms of their temporal variability, spatial patterns, and influences on ENSO.

Section 2 introduces the datasets, indices, and statistical methods employed. Section 3 compares the spatiotemporal features of the SPQ and SPMM. Section 4 examines the differences between the influences of the SPQ and SPMM on ENSO. Section 5 compares the connections of the SPQ and SPMM with ENSO in the Coupled Model Intercomparison Project Phase 5 (CMIP5) preindustrial/industrial simulations. Finally, section 6 provides a summary and discussion of our results.

2. Data and Methods

2.1. Observed and Modeled Datasets

For atmospheric variables, we use the monthly mean sea-level pressure (SLP) and 10-m wind data from the National Centers for Environmental Prediction/National Center for Atmospheric Research project (Kalnay et al., 1996), which cover the period 1948–2017. The SST data over the same period are from the Met Office Hadley Centre Sea Ice and Sea Surface Temperature dataset (Rayner et al., 2006). The subsurface ocean temperature data (1948–2017) originate from the Institute of Atmospheric Physics ocean gridded products (Cheng et al., 2017), which feature global coverage of the oceans at 1° × 1° horizontal resolution on 41 vertical levels from 1 to 2,000 m.

For coupled climate model output, we employ historical simulations (with externally varying forcings; 1948–2005) from the 23 CMIP5 climate models (Taylor et al., 2012) to examine whether or not the models simulated different relationships of the SPQ and SPMM with ENSO. The details and references of models are summarized in the supporting information, Table S1. To examine the possible contribution of internal climate variability alone to the SPQ/SPMM-ENSO relationships, the last 100 years of the preindustrial simulations (with the external forcing fixed at the preindustrial level) from the 23 CMIP5 models were also analyzed. All atmospheric and oceanic fields from the models are regridded onto a common 1° × 1° latitude-longitude grid for ease of comparisons between models.

For all atmospheric and oceanic variables in observations, monthly mean anomalies are defined as departures from 30-year calendar monthly means (1981–2010) after removing the linear trend. Several statistical methods, including regression, correlation, and composite analyses, are utilized in this study. The significance of regression, correlation, and composite values was tested by a two-tailed Student's *t* test.

2.2. Definitions of Indices

Following Ding, Li, and Tseng (2015), the SPQ index is obtained by calculating the difference between the sum of normalized SSTAs over two positive poles ([58–36°S, 173–145°W] and [37–17°S, 103–76°W]) and the sum of normalized SSTAs over two negative poles ([47–25°S, 142°E–179°W] and [59–40°S, 113–81°W]) (see Figure 1a). These four poles where the SPQ index is defined correspond closely to the four loading centers of the second empirical orthogonal function (EOF2) mode of SSTAs in the extratropical South Pacific (Ding, Li, & Tseng, 2015).

Following Zhang, Clement, and Di Nezio (2014), we use the simple SSTA index (referred to as the SPMM-1_{SST} index; SST averaged over the subtropical southeast Pacific [25–15°S, 110–90°W]) to represent the SPMM variability. In addition, we also obtain the SPMM index (SPMM-2) following the methodology of You and Furtado (2018). Maximum covariance analysis is applied to the cross-covariance matrix between SST and 10-m wind anomalies in the subtropical southeast Pacific (35–10°S, 180–70°W). To exclude the ENSO influence from the analysis result, we linearly remove the contemporaneous cold tongue index (CTI; SST averaged over [6°S–6°N, 180–90°W]) from the fields month by month prior to the maximum covariance analysis. This SPMM mode accounts for 20.6% of the total coupled variance and is well separated from higher modes according to the criterion of North et al. (1982). The normalized SST and 10-m wind expansion coefficients associated with the SPMM are referred to as the SPMM-2_{SST} and SPMM-2_{wind} indices, respectively.

3. Spatiotemporal Features of the SPQ and SPMM

To illustrate the different spatial features between the SPQ and SPMM and their different linkages with the large-scale circulation variability, we regress Pacific SST, SLP, and 10-m wind anomalies onto the SPQ and SPMM-1_{SST} indices, respectively (Figures 1a and 1b). We note that the SPQ-related SSTA signature in the South Pacific resembles the SPMM-related SSTA pattern, with their related negative (positive) SSTAs overlapping over the southwest Pacific off the east coast of Australia (over the subtropical southeast Pacific off the west coast of Chile). However, there are remarkable differences between their related SSTA patterns. The SPQ exhibits a zonal SSTA pattern with four centers over the South Pacific, while the SPMM exhibits a tilted northeast-southwest-oriented meridional SSTA structure in the South Pacific. SSTAs associated with the SPMM have large amplitudes mainly confined to the subtropical southeast Pacific, and they have smaller amplitudes than those associated with the SPQ over the southwest Pacific off the east coast of Australia as well as over high latitudes of the South Pacific. These differences are generally consistent with the fact that the SPQ (SPMM) is defined over the whole extratropical South Pacific basin (only over the subtropical southeast Pacific). Therefore, in contrast to the local SST mode of the SPMM in the subtropical southeast Pacific, the SPQ, as a basin-scale South Pacific SST mode, has its own characteristic SSTA pattern.

The SPMM-related SLP anomaly (SLPA) pattern shows a northeast-southwest-oriented dipole-like structure with opposite-sign SLPAs over the high-latitude South Pacific and the mid-latitude southeast Pacific, consistent with previous findings that have attributed the SPMM's atmospheric forcing pattern to a northeast-southwest-oriented SLPA dipole with a nodal point near 50°S (Zhang, Clement, & Di Nezio, 2014; You and Furtado, 2018). According to You and Furtado (2018), the northern pole of this SLPA dipole alters the strength of the South Pacific subtropical high and in turn modulates the climatological southeasterly trade winds, thereby generating positive SSTAs in the subtropical southeast Pacific. In contrast, the SPQ is linked to a zonal wavenumber-3 SLPA pattern extending from the southwest Pacific to the southeast Pacific off the west coast of Chile. Qin et al. (2017) reported that this wavenumber-3 structure of SLPAs associated with the SPQ is significantly correlated with both the Southern Annular Mode (SAM) and the second Pacific-South American (PSA2) mode. As a consequence of the wavenumber-3 structure, SLPAs associated with the SPQ have larger amplitudes than those associated with the SPMM over the mid-latitude southwest Pacific as well as over high latitudes of the South Pacific. This difference between the SPQ- and SPMM-related SLPA patterns is consistent with the difference between their related SSTA patterns. The large-

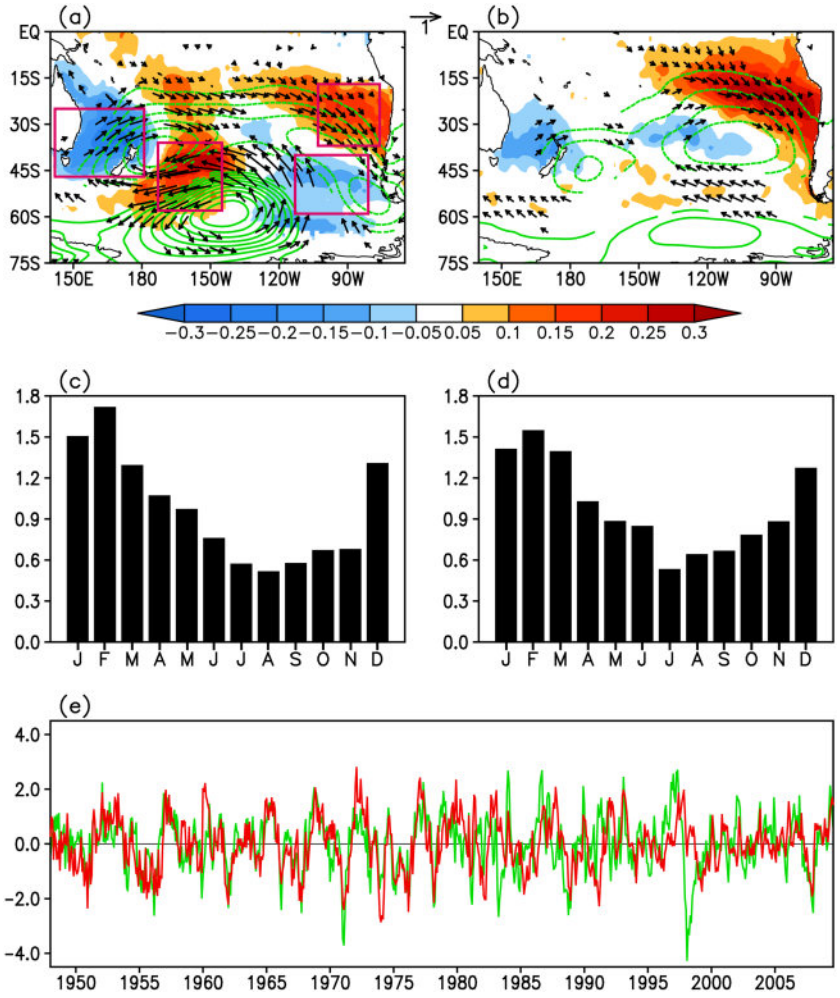

Figure 1. (a) Regression of anomalies of monthly SST (°C; shaded), SLP (hPa; contours), and 10-m wind (m s^{-1}; vectors) onto the monthly SPQ index. The contour interval is 0.15 hPa for SLPA (positive, solid; negative, dashed), and the reference wind vector is 1 m s^{-1}. Only SST, SLP, and 10-m wind anomalies significant at the 95% confidence level according to a two-tailed Student's *t* test are shown. (b) As in (a), but for regression onto the monthly SPMM-1_{SST} index. (c) Seasonal variations of the standard deviation of the monthly SPQ index. (d) As in (c), but for the monthly SPMM-1_{SST} index. (e) The normalized monthly SPQ (blue line) and SPMM-1_{SST} (red line) indices as functions of time. In (a), four pink boxes (from left to right: [47–25°S, 142°E–179°W]; [58–36°S, 173–145°W]; [59–40°S, 113–81°W]; and [37–17°S, 103–76°W]) define the locations of the four poles of the SPQ.

amplitude negative and positive SLPAs over the mid-latitude southwest Pacific and high-latitude South Pacific, respectively, associated with the SPQ favor the development of significant negative and positive SSTAs over the southwest Pacific, thereby leading to large-amplitude SSTAs in the region. As noted by Zheng and Wang (2017), in addition to the wind anomalies associated with the PSA pattern that influence the quadrupole SST pattern through changes in surface heat fluxes, the cloud-related radiations are also important to the formation of the SPQ pattern.

The SPQ and SPMM-1_{SST} indices show similar seasonal variations, with the maximum variance during austral summer (December–March [DJFM]) and minimum variance during austral winter (July–September [JAS]) (Figures 1c and 1d). Conversely, previous studies have reported that the atmospheric variability associated with the SPQ (i.e., the wavenumber-3 structure of SLPAs) and SPMM (the SPMM-2_{wind} index) peaks during austral winter (Ding, Li, & Tseng, 2015; You and Furtado, 2018). You and Furtado (2018) attributed the out-of-phase seasonality of the SPMM SST and wind components to the seasonal cycle of the mixed layer depth (MLD), which is usually shallowest during austral summer and deepest during austral winter in the South Pacific. The shallow MLD tends to strengthen the SPMM-associated WES feedback, thus resulting

Table 1
Classification of Years in Which Positive (Negative) SPQ Events Are or Are Not Simultaneous With a Positive (Negative) SPMM Event During the Period 1948–2017 (See Text for the Definition of SPQ and SPMM Events).

	Positive SPMM	Neutral SPMM	Negative SPMM
Positive SPQ	1952, 1957, 1965, 1977, 1993, 2012, 2017	1969, 1979, 1984, 1987, 1997, 2002	1991
Neutral SPQ	1953, 1960, 1972, 1983, 1992, 2016	1948, 1949, 1950, 1951, 1958, 1959, 1961, 1963, 1964, 1968, 1970, 1980, 1985, 1986, 1988, 1989, 1990, 1994, 1995, 1996, 2000, 2001, 2003, 2004, 2005, 2006, 2007, 2008, 2009, 2010, 2013, 2014, 2015	1967, 1974, 1976, 1982, 1999, 2011
Negative SPQ		1954, 1955, 1956, 1966, 1973, 1981, 1998	1962, 1971, 1975, 1978

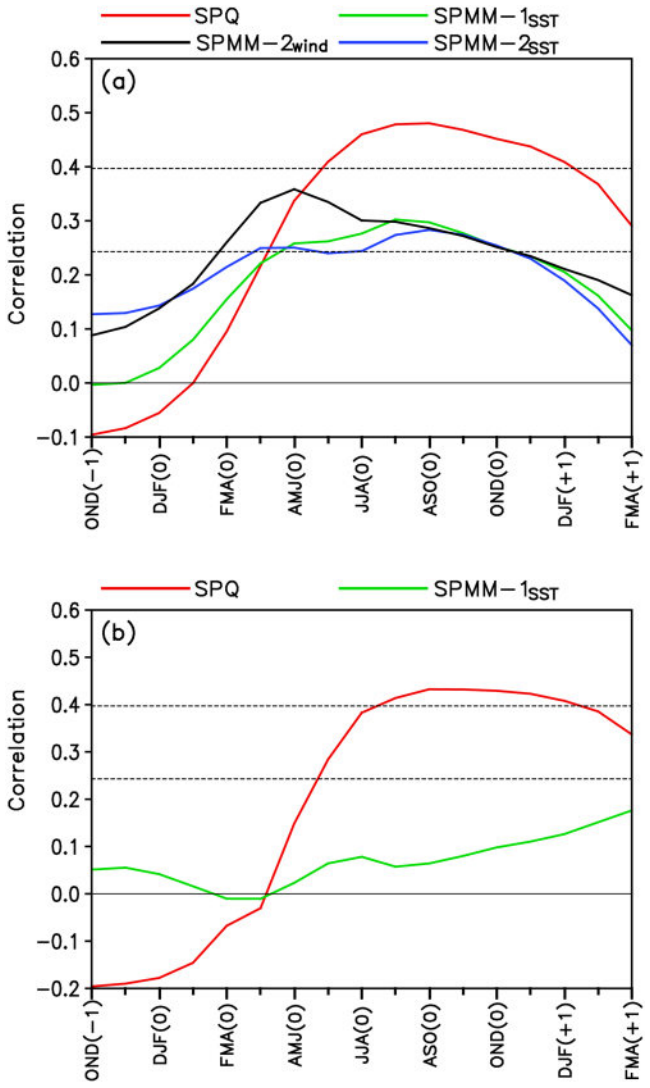

Figure 2. (a) Cross-correlations of the austral summer (JFM-averaged) SPQ, SPMM-1_{SST}, SPMM-2_{SST}, and SPMM-2_{wind} indices with 3-month averaged CTI. The year in which ENSO develops is denoted as year(0) and the preceding and following years as year(−1) and year(+1), respectively. (b) Partial cross-correlation between the austral summer SPQ (SPMM-1_{SST}) index and 3-month averaged CTI by linearly removing the austral summer SPMM-1_{SST} (SPQ) index. In (a) and (b), the horizontal dashed lines show the 95% and 99.9% confidence levels, respectively.

in the peak of the SPMM SST variability occurring during austral summer. Ding, Li, and Tseng (2015) also demonstrated that the SPQ-related SST response to atmospheric forcing could be intensified due to the shallow MLD in the extratropical South Pacific during austral summer, thus resulting in the maximum variance of the SPQ variability occurring during austral summer.

The correlation coefficient between the monthly SPQ and SPMM-1_{SST} indices is 0.51 (significant at the 99.9% confidence level). This suggests a close connection between the SPQ and SPMM variations (Figure 1e). However, although the SPQ index is significantly correlated with the SPMM index, the fluctuations of the SPQ are not completely consistent with those of the SPMM, and the SPQ also possesses its own variability independent of the SPMM. To demonstrate this, all years in the period 1948–2017 are classified as strong SPQ or SPMM years, or neutral years. A strong SPMM (SPQ) year is defined as a year in which the SPMM-1_{SST} (SPQ) index at its peak phase (JFM) is larger than 1.0 standard deviation. We note that there are only 7 of 14 strong positive SPQ years occurring simultaneously with strong positive SPMM years (Table 1). In particular, 1991 was a year in which the SPMM-1_{SST} index is −1.57, while the SPQ index was 1.02 (a strong positive SPQ year). Similarly, only 4 of 11 strong negative SPQ years occur simultaneously with strong negative SPMM years, while the remaining 7 strong negative SPQ years are accompanied by neutral SPMM years. These results support the relative independence of the SPQ and SPMM.

4. Relationships of the SPQ and SPMM with ENSO

The results presented above have shown that there are differences between the spatial patterns and temporal variability of the SPQ and SPMM. These differences may result in different climate effects. We next turn our attention to the relationships of the SPMM and SPQ with ENSO. We compute the cross-correlations between the JFM-averaged SPQ index and 3-month mean CTI and between the JFM-averaged SPMM-1_{SST} index and 3-month mean CTI (Figure 2a). For the SPQ, the peak correlation with ENSO occurs during August–October (ASO), about 7 months after the peak of the SPQ during JFM. This result is consistent with the findings of Ding, Li, and Tseng (2015). The correlation of the SPMM-1_{SST} index similarly peaks around ASO, but the peak correlation between the SPMM-1_{SST} index and CTI is much weaker than that between the SPQ index and CTI. In addition, we also calculated the lead-lag correlations of

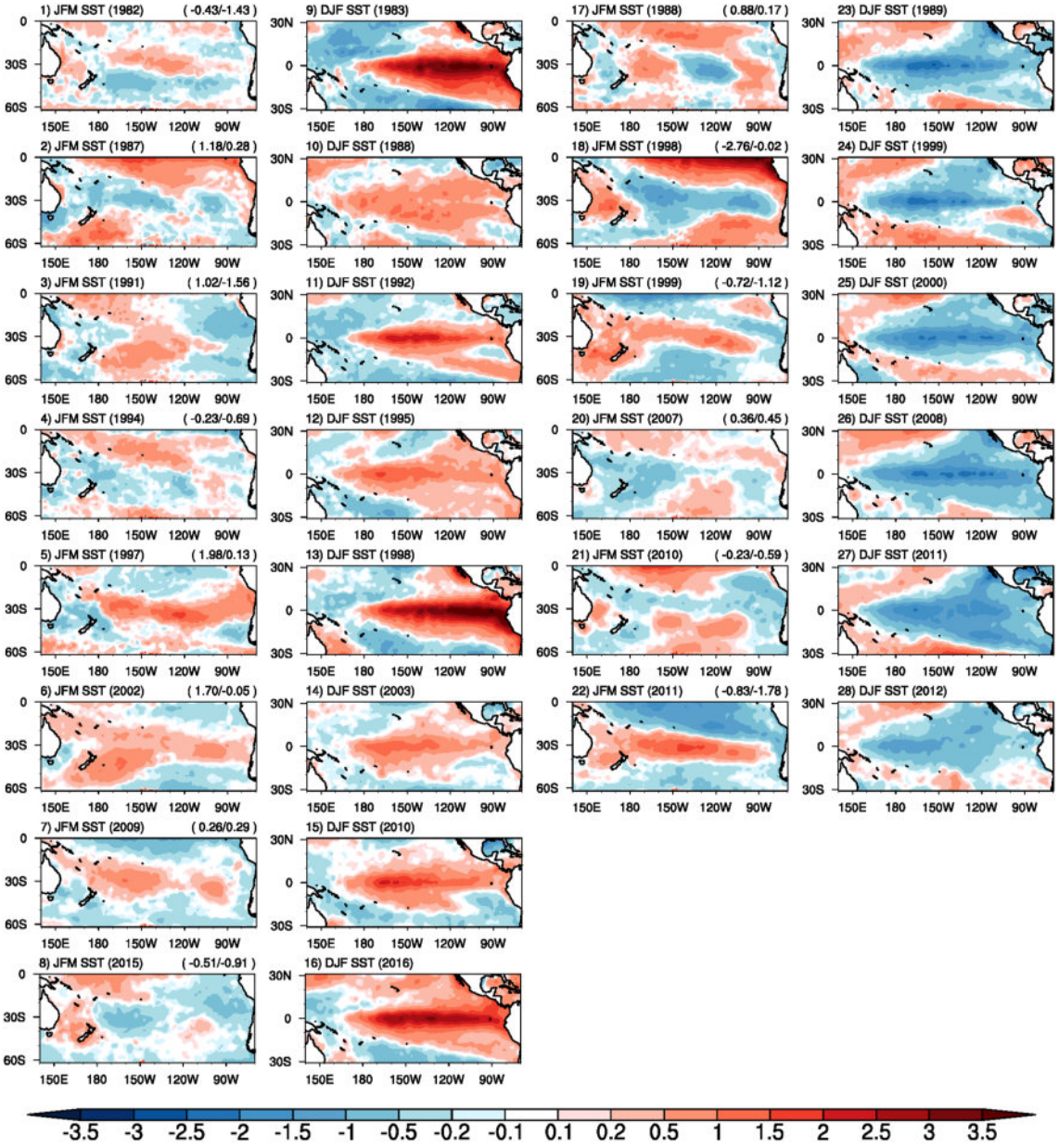

Figure 3. Panels (1–8): The JFM-averaged SSTA precursors to the moderate to strong El Niño events occurring between 1980 and 2017. Panels (9–16): DJF-averaged SSTAs for these El Niño events. Panels (17–22): The JFM-averaged SSTA precursors to the moderate to strong La Niña events occurring between 1980 and 2017. Panels (23–28): DJF-averaged SSTAs for these La Niña events. In the Panels (1–8) and (17–22), also shown on top of each panel is the SPQ and SPMM indices.

the SPMM-2_{SST} and SPMM-2_{wind} indices with the CTI for comparison. The peak correlation between the SPMM-2_{SST} (SPMM-2_{wind}) index and CTI occurs during ASO (AMJ) and is again much weaker than the peak correlation of the SPQ index with CTI during ASO. The SPQ index shows larger correlations than both the SPMM-2_{SST} and SPMM-2_{wind} indices with the CTI for lead times of up to a year. The peak correlation of the SPMM-2_{wind} index with the CTI occurs about 3 months prior to that of the SPMM-2_{SST} index, which is almost consistent with the fact that the SPMM-2_{wind} index leads the SPMM-2_{SST} index about 1–2 months (You and Furtado, 2018).

To further examine the relative importance of the SPQ and SPMM to ENSO, we compute the partial cross-correlation between the austral summer SPQ (SPMM-1_{SST}) index and 3-month averaged CTI by linearly removing the austral summer SPMM-1_{SST} (SPQ) index (Figure 2b). With the removal of the SPMM effect,

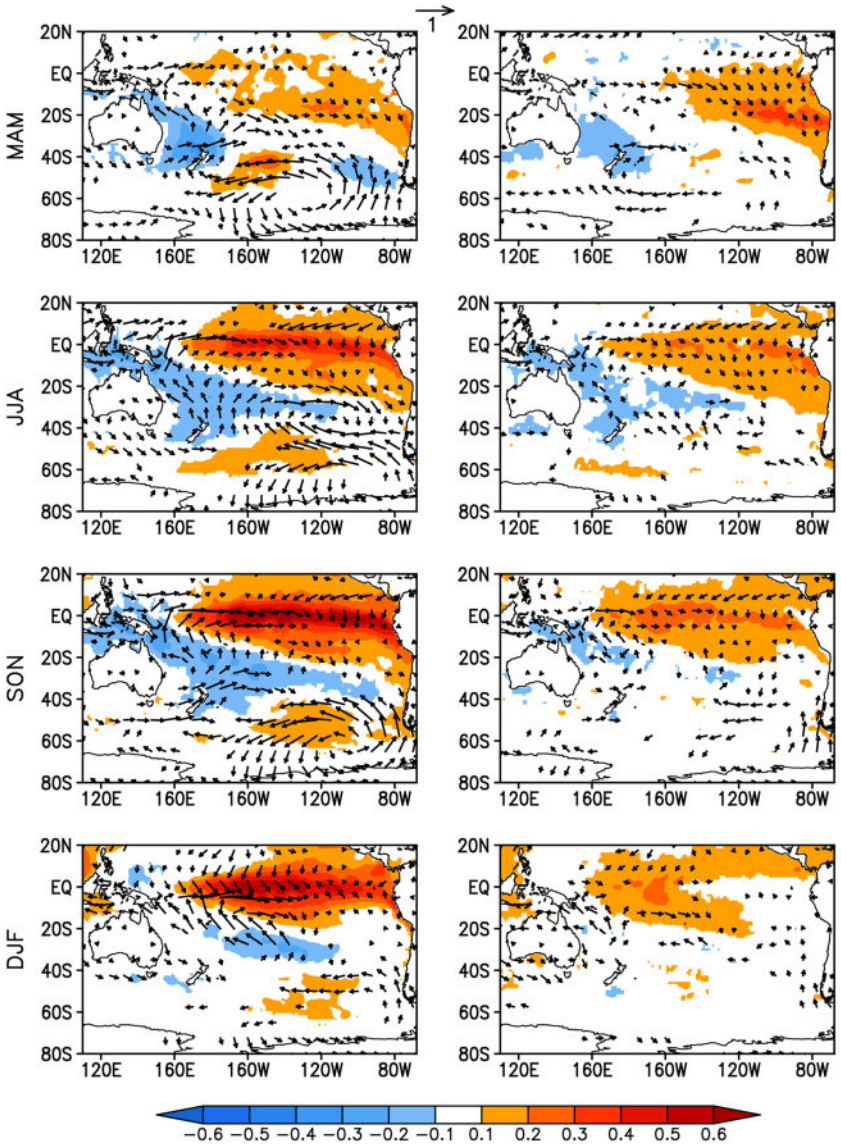

Figure 4. Regressions of the observed 3-month averaged SST (°C; shaded) and surface wind anomalies (m s^{-1}; vectors) onto the JFM-averaged SPQ (left panel) and SPMM-1_{SST} (right panel) indices for several lead times (MAM, JJA, SON, and DJF). Positive (red) and negative (blue) SST anomalies, significant at the 95% confidence level, are shaded. Only surface wind vectors significant at the 95% confidence level are shown.

the correlations between the SPQ and CTI are slightly reduced but still significant at or above the 99.9% confidence level for lead times longer than a few months. In contrast, with the removal of the SPQ effect, the correlations between the SPMM-1_{SST} index and CTI are greatly reduced, and their peak correlation during ASO is no longer significant.

The above analyses indicate that that the SPQ may be more closely related than the SPMM to ENSO. This leads us to speculate that compared with the SPMM, the SPQ may represent an improved precursor signal than the SPMM for ENSO events. To demonstrate this, we examine in detail the South Pacific SSTA precursors for the moderate to strong El Niño events occurring between 1980 and 2017 (Figure 3). The definition of the moderate to strong El Niño events was provided by the Climate Prediction Center (available at https://origin.cpc.ncep.noaa.gov/products/analysis_monitoring/ens-ostuff/ONI_v5.php). We note that the 1987, 1991, 1997, and 2002 SSTA precursors all display the SPQ signatures. Specifically, about 50% of these moderate to strong El Niño events (four out of eight events) were preceded by SPQ events (with the SPQ index

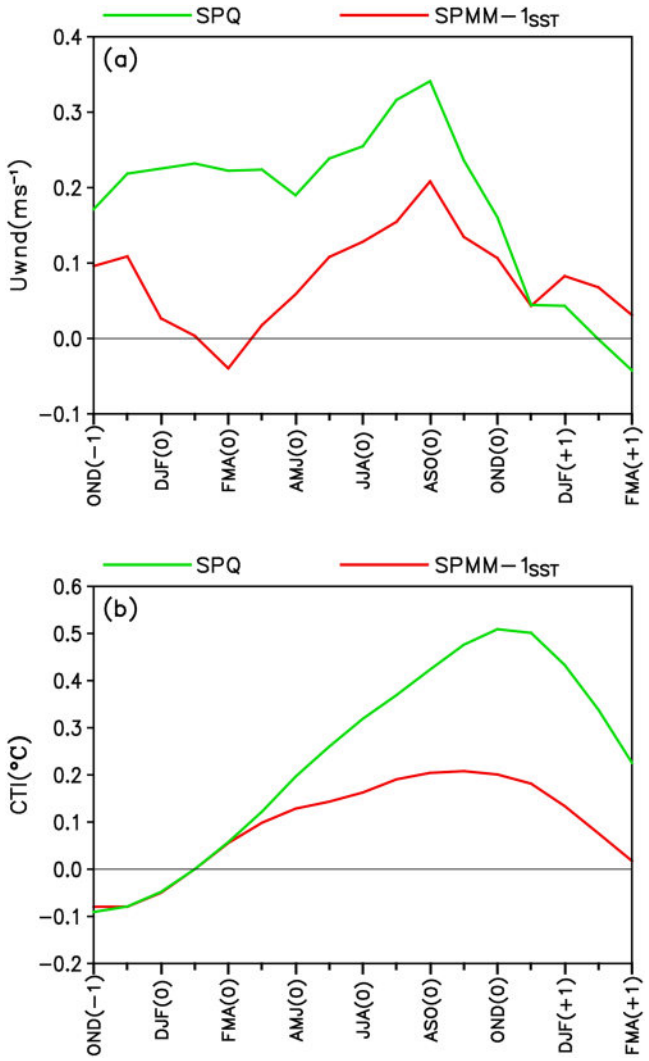

Figure 5. (a) Lead-lag regression coefficients of the 3-month running mean surface zonal wind anomalies area-averaged over the western-central equatorial Pacific (5°S–5°N, 120–160°E) onto the JFM-averaged SPQ and SPMM-1_{SST} indices. (b) Lead-lag regression coefficients of the 3-month running mean CTI onto the JFM-averaged SPQ and SPMM-1_{SST} indices. In (a) and (b), the year in which ENSO develops is denoted as year(0) and the preceding and following years as year(−1) and year(+1), respectively.

greater than 1.0). However, the SPMM index is less than 1.0 for all these El Niño events and even shows a large negative value for several El Niño events. In addition, we also examine the South Pacific SSTA precursors for the moderate to strong La Niña events occurring between 1980 and 2017 (see also Figure 3). We note that the JFM-averaged SPQ index prior to the 1999 La Niña event is −2.76, while the JFM-averaged SPMM index is only −0.02. Although the JFM-averaged SPMM index prior to the 2000 and 2012 La Niña events is less than −1.0, the SPQ index is also relatively small (≤0.5) for these two events. Therefore, generally speaking, it seems that compared with the SPMM, the SPQ may act as an improved precursor signal than the SPMM for El Niño/La Niña events.

To understand why the SPQ is more closely linked than the SPMM to ENSO, we examine the evolutions of 3-month averaged surface wind and SST anomalies regressed on the JFM-averaged SPQ and SPMM-1_{SST} indices (Figure 4). During MAM (March–May), the quadrupole-like SSTA pattern associated with the SPQ can still be clearly seen in the South Pacific. At this moment the SPQ-related SSTA pattern in the subtropical southeast Pacific resembles a SPMM pattern, with significant positive SSTAs in the subtropical southeast Pacific. In addition, the SPQ-related significant negative SSTAs can also be found in the subtropical southwest Pacific off the north and east coast of Australia. These negative SSTAs, combined with positive SSTAs in the central-eastern equatorial Pacific originating from the subtropical southeast Pacific via the positive WES feedback (Xie & Philander, 1994), could induce westerly wind anomalies in the western equatorial Pacific. These westerly wind anomalies can act as an efficient trigger for the Bjerknes feedback (Bjerknes, 1969) that drives the development of an El Niño event during subsequent seasons. During DJF, an El Niño-like pattern is well developed in the tropical Pacific.

In contrast, SSTAs associated with the SPMM are characterized by large-amplitude positive SST anomalies mainly confined to the subtropical southeast Pacific during MAM, and they gradually extend into the central-eastern equatorial Pacific through the WES feedback during JJA (June–August) (Zhang, Clement, & Di Nezio, 2014). SSTAs associated with the SPMM are relatively weak in the subtropical southwest Pacific during MAM, and they do not extend far into the deep tropics during JJA. As a result, westerly wind anomalies associated with the SPMM are relatively large in the central-eastern equatorial Pacific during MAM and JJA, and they are much weaker than those associated with the SPQ in the western equatorial Pacific (see also Figure 5a). This is consistent with the results of Zhang, Clement, and Di Nezio (2014), who found that the SPMM exhibits a much greater impact on the central-eastern equatorial Pacific than on the western equatorial Pacific. Given those westerly wind anomalies in the western equatorial Pacific are considered essential for the occurrence of an El Niño event, the weaker westerly wind anomalies associated with the SPMM are less favorable for the development of positive SSTAs in the central-eastern equatorial Pacific. As a result, the warming there is not well developed and instead starts to decay during DJF (Figures 4 and 5b).

The above analyses suggest that the SPQ-related SSTAs in the subtropical southwest Pacific can directly induce the westerly wind anomalies in the western equatorial Pacific and may also play an important role in the development of ENSO events. To further test this idea, we compute the partial regressions of the seasonally averaged surface wind and SST anomalies onto the JFM-averaged SPQ index by removing the effect of the SPMM-1_{SST} index (Figure 6). With the removal of the SPMM effect, the SPQ-related significant positive SSTAs in the subtropical southeast Pacific become indistinct during MAM, and the SPQ-related quadrupole SSTA pattern changes into a tripole-like pattern, characterized by negative-positive-negative SSTAs

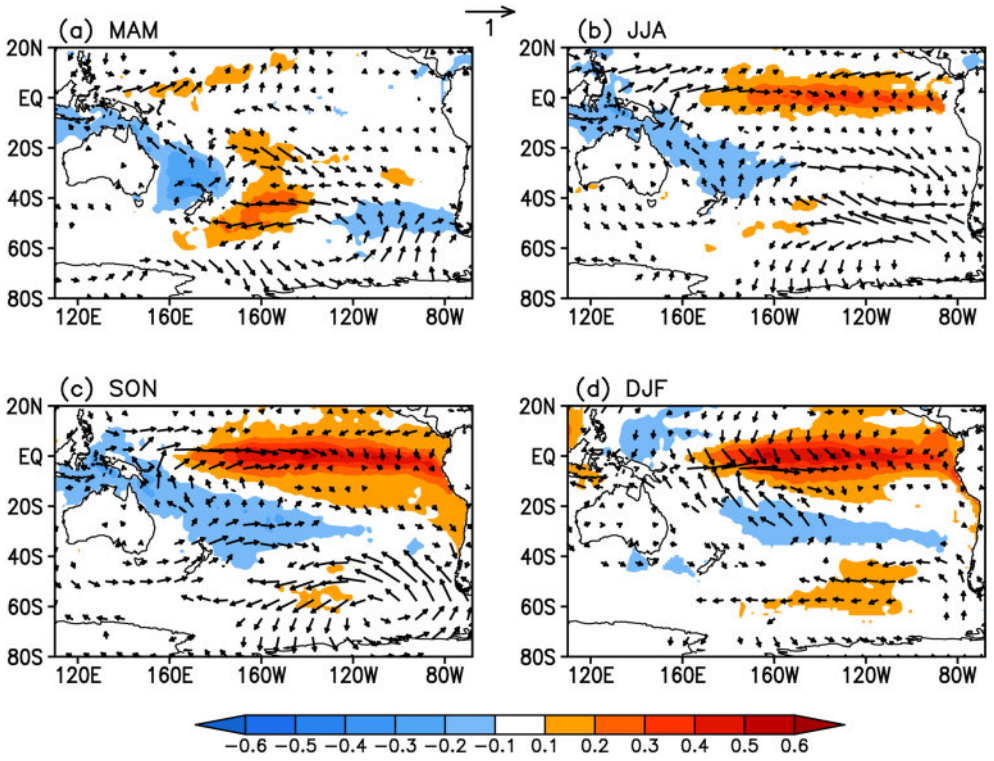

Figure 6. Partial regressions of the observed 3-month averaged SST (°C; shaded) and surface wind anomalies (m s^{-1}; vectors) onto the JFM-averaged SPQ index by removing the linear effect of the SPMM-1_{SST} index for several lead times [(a) MAM, (b) JJA, (c) SON, and (d) DJF]. Positive (red) and negative (blue) SST anomalies, significant at the 95% confidence level, are shaded. Only surface wind vectors significant at the 95% confidence level are shown.

stretching from the southwest Pacific off the east coast of Australia to the high-latitude southeast Pacific. At this time, significant westerly wind anomalies induced by negative SSTAs in the southwest Pacific can still be clearly seen in the western-central equatorial Pacific, which ultimately lead to a distinct El Niño-like pattern during the following DJF season via the Bjerkness feedback process. In comparison, the amplitude of positive SSTAs in the eastern equatorial Pacific with the removal of the SPMM effect (Figure 6) is slightly less than the warming amplitude without the removal of the SPMM effect but greater than the warming amplitude associated with the SPMM (Figure 4). These results suggest that in addition to SSTAs in the subtropical southeast Pacific, SSTAs over the other three poles of the SPQ (especially SSTAs in the subtropical southwest Pacific) associated with the SPQ may contribute substantially to the development of ENSO events.

Furthermore, we compute the cross-correlations with 3-month averaged CTI of the JFM-averaged SSTAs area-averaged over each of the four poles where the SPQ index is defined (Figure 7). For two- to three-season lead times, the correlations between SSTAs over the southwest Pacific (Pole A [47–25°S, 142°E–179°W]) and CTI are comparable to (but slightly higher than) those between SSTAs over the southeast Pacific (Pole D [37–17°S, 103–76°W]) and CTI. In addition, SSTAs over the high-latitude South Pacific (Pole B [58–36°S, 173–145°W] and Pole C [59–40°S, 113–81°W]) also exhibit significant correlations for lead times of up to a year. The peak correlation of SSTAs over all the four poles is lower than that of the SPQ index. These results are generally consistent with the findings of several previous studies that have considered the SSTAs in the southwest Pacific, SSTAs in the southeast Pacific, or a zonal SST dipole over the high-latitude South Pacific as a precursor to ENSO (Holbrook & Bindoff, 1997; Toniazzo, 2010; Ballester et al., 2011; Zhang, Clement, & Di Nezio, 2014, Zhang, Deser, et al., 2014). However, we argue that the SPQ, as a basin-scale SSTA pattern over the South Pacific, includes all the effects of SSTAs in the southwest Pacific, the southeast Pacific, and the high-latitude South Pacific, unlike the SPMM pattern that mainly underlines the importance of the SSTAs in the southeast Pacific to the ENSO development. Therefore, in contrast to the SPMM, the SPQ is more closely related to ENSO and may provide a more effective precursor signal to ENSO.

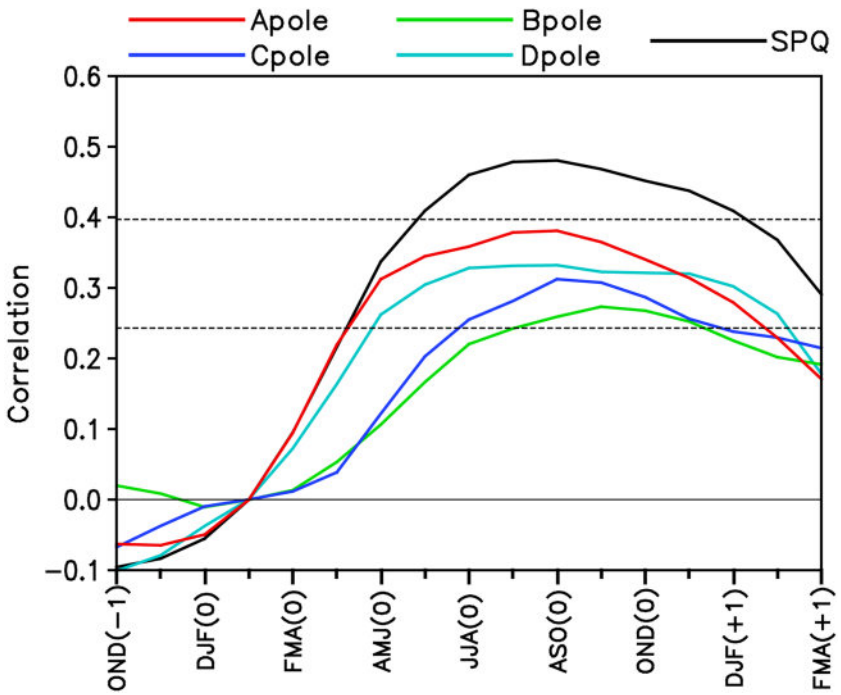

Figure 7. Cross-correlations of the austral summer (JFM-averaged) SPQ index and SSTAs area-averaged over each of four poles (Pole A [47–25°S, 142°E–179°W], Pole B [58–36°S, 173–145°W], Pole C [59–40°S, 113–81°W], and Pole D [37–17°S, 103–76°W]), where the SPQ index is defined with 3-month averaged CTI. The year in which ENSO develops is denoted as year(0) and the preceding and following years as year(−1) and year(+1), respectively. The horizontal dashed lines show the 95% and 99.9% confidence levels, respectively.

We further compare the evolutions of subsurface temperature anomalies associated with the SPQ and SPMM (Figure 8). For the SPQ, there are significant positive subsurface temperature anomalies in the central Pacific during MAM, which appear to be excited by anomalous westerly winds in the western equatorial Pacific that may force downwelling equatorial Kelvin waves and cause a deepening of the thermocline in the central Pacific. After MAM, the positive subsurface temperature anomalies associated with the SPQ extend to the eastern Pacific during JJA when they tend to intensify the surface warming there. For the SPMM, however, there are only weak (not significant) positive subsurface temperature anomalies in the central Pacific during MAM. They intensify but remain almost stationary with only a slight eastward propagation during subsequent seasons, thereby limiting the warming in the eastern equatorial Pacific.

The foregoing analysis suggests that the thermocline-SST coupling process is important in developing subsequent El Niño events for the SPQ but not for the SPMM. This is consistent with the findings of Matei et al. (2008), who reported that the subtropical southeast Pacific influences the tropical Pacific mainly through the ocean-atmosphere mixed layer interaction. This is further supported by the findings of Zhang, Clement, and Di Nezio (2014), who reproduced the influence of the SPMM on ENSO using just an atmospheric general circulation model (AGCM) coupled to a slab ocean mixed layer model (AGCM-slab model). In contrast, the SPQ influence on ENSO involves the dynamical thermocline-SST feedback process, which makes important contributions to the development of ENSO. In contrast to SSTAs in the southeast Pacific that may exert effects on ENSO primarily through the thermodynamics, SSTAs in the southwest Pacific could contribute more directly to the oceanic Kelvin wave activity (as a response to westerly wind anomalies) in the western tropical Pacific and hence the Bjerknes dynamical feedback. This further highlights the important role of SSTAs in the southwest Pacific in developing ENSO.

5. CMIP5 Multimodel Outputs

The above suggests that the SPQ is more closely linked to ENSO than the SPMM. Further analyses of the CMIP5 multimodel outputs support the observational results. The names of 23 CMIP5 models utilized in this study are listed in Table S1. Most of the CMIP5 models are able to reproduce reasonably well the spatial

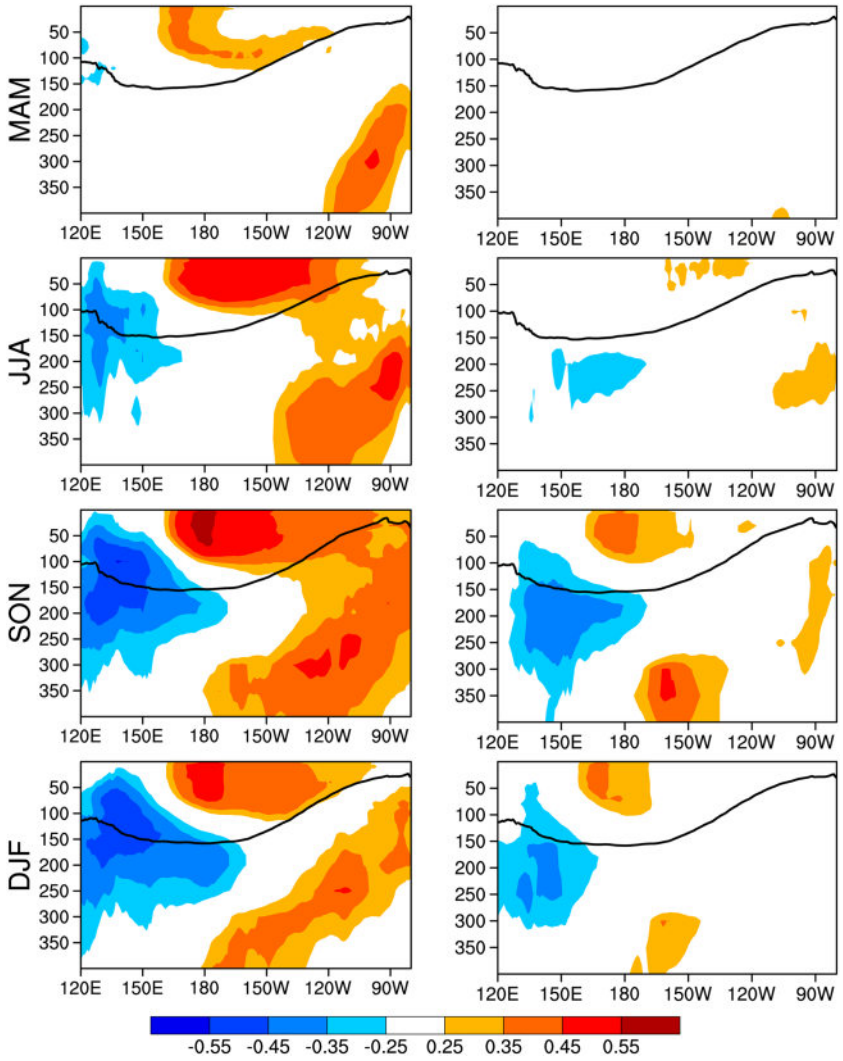

Figure 8. Correlation maps of the JFM-averaged SPQ (left panel) and SPMM-1_{SST} (right panel) indices with the 3-month averaged ocean subsurface temperature anomalies at different depths in meters averaged over 5°S–5°N for several lead times (MAM, JJA, SON, and DJF). Positive (red) and negative (blue) ocean subsurface temperature anomalies, significant at the 95% confidence level, are shaded. Thick black contour indicates the climatological position of the 23 °C isotherm.

patterns of the SPQ and SPMM, and the spatial correlations between the simulated and observed SPQ (SPMM) are larger than 0.60 (0.67) for all the CMIP5 models (see Figures S1 and S2).

Figure 9a shows the correlations of the JFM-averaged SPQ and SPMM-1_{SST} indices with the following ASO-averaged CTI in the historical simulations from the 23 CMIP5 models. We found that the correlations between the SPQ index and CTI are higher than those between the SPMM-1_{SST} index and CTI in most of the CMIP5 models (16 of 23 CMIP5 models). The multimodel ensemble of climate models shows that the SPQ has a stronger correlation than the SPMM with ENSO with a lead time of about 7 months. Note, however, that only 7 (3) CMIP5 models reproduce the significant lagged correlation between the SPQ (SPMM) and ENSO. This shows that, in general, the influence of the SPQ or SPMM on ENSO may be underestimated in the CMIP5 models.

The above analysis compares the relationships of the SPQ and SPMM with ENSO in the CMIP5 historical simulations. It further indicates that the lagged relationship between the SPQ and ENSO is more robust than the relationship between the SPMM and ENSO. Next, we examine the relationships of the SPQ and SPMM

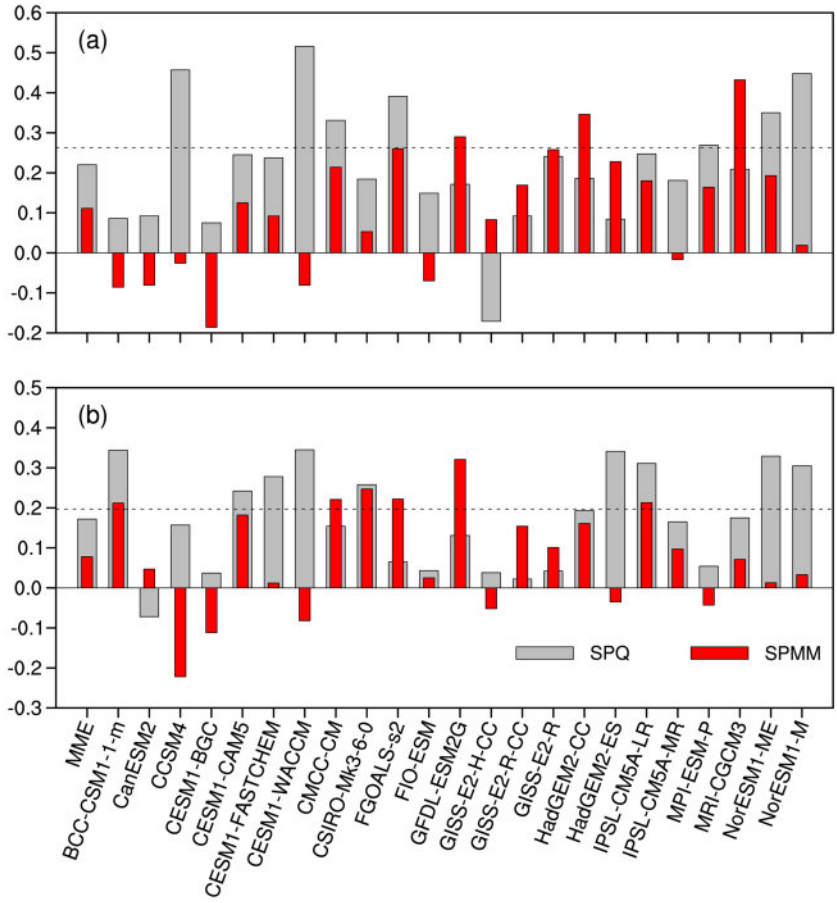

Figure 9. (a) Correlations of the JFM-averaged SPQ and SPMM-1_{SST} indices with the following ASO-averaged CTI in the historical simulations from the 23 CMIP5 models. Also shown is the multimodel ensemble (MME) of 23 CMIP5 models. The horizontal dashed line shows the 95% confidence level. (b) As in (a) but for the preindustrial simulations from the 23 CMIP5 models.

with ENSO in the CMIP5 preindustrial simulations (Figure 9b). In the preindustrial simulations, the correlations between the SPQ index and CTI are also higher than those between the SPMM-1_{SST} index and CTI in most of the CMIP5 models (17 of 23 CMIP5 models). These results from the preindustrial simulations are very similar to those from the historical simulations, which provide further evidence that the SPQ seems to be more closely related to ENSO than the SPMM. As shown in Figure 10a, the CMIP5 models that have a higher correlation between SPMM and ENSO in the historical simulations generally tend to show a stronger correlation between SPMM and ENSO in the preindustrial simulations, suggesting that interval variability may play an important role in the SPMM-ENSO relationship. Similar results can be obtained for the SPQ-ENSO relationship (Figure 10b).

To stress the importance of SSTAs over the southwest Pacific to ENSO, we also computed the correlations of the JFM-averaged SSTAs over the southwest Pacific (47–25°S, 142°E–179°W) with the following ASO-averaged CTI in the preindustrial simulations from the 23 CMIP5 models. The correlations of SSTAs over the southwest Pacific are generally comparable to those of SSTAs over the southeast Pacific (37–17°S, 103–76°W) in most of the CMIP5 models (Figure S3). In addition, it is interesting to note that the simulated lagged correlation between the SPQ and ENSO (denoted as R_1) is closely associated with the correlation between SSTAs over the southwest Pacific and ENSO (denoted as R_2) (Figure 10c). The CMIP5 models that produce a higher correlation between SSTAs over the southwest Pacific and ENSO tend to show a stronger correlation between SPQ and ENSO. The correlation between R_1 and R_2 is as high as −0.69 across the 23 CMIP5 models. However, a similar robust relationship cannot be found between

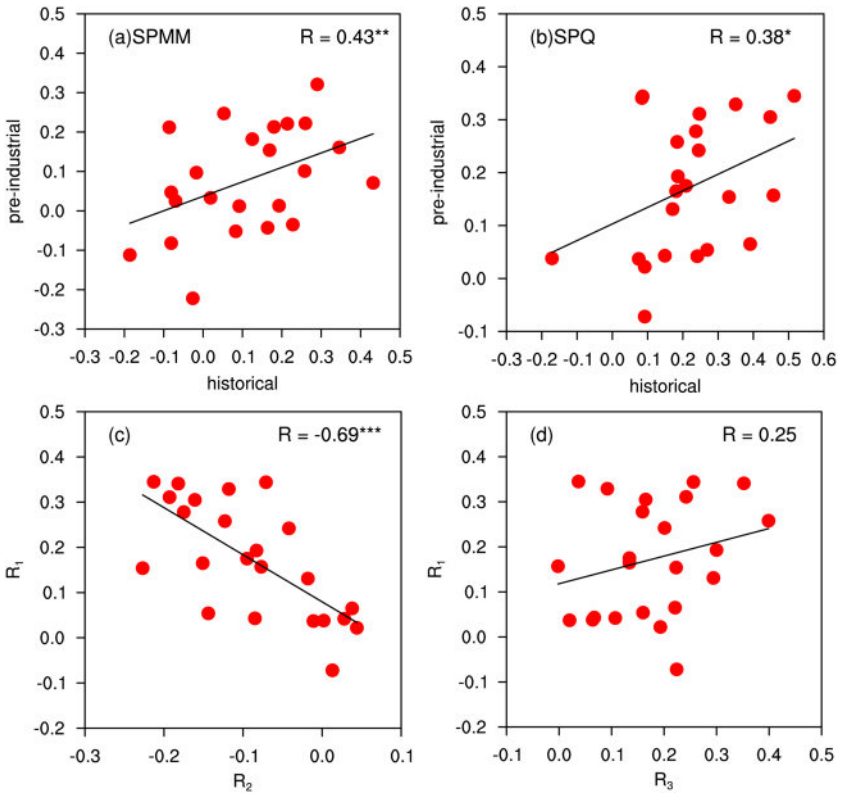

Figure 10. (a) Scatter plots for the SPMM-ENSO correlation between the CMIP5 historical and preindustrial simulations. (b) Scatter plots for the SPQ-ENSO correlation between the CMIP5 historical and preindustrial simulations. (c) Scatter plots for the CMIP5 preindustrial simulations between the SPQ-ENSO correlation (denoted as R_1) and the correlation between SSTAs over the southwest Pacific (47–25°S, 142°E–179°W) and ENSO (denoted as R_2). (d) Scatter plots for the CMIP5 preindustrial simulations between the SPQ-ENSO correlation (denoted as R_1) and the correlation between SSTAs over the southeast Pacific (37–17°S, 103–76°W) and ENSO (denoted as R_3). The best fit is represented by the solid line, and *, **, and *** indicate the 90%, 99%, 99.9% confidence level, respectively.

the SPQ-ENSO correlation (denoted as R_1) and SSTAs over the southeast Pacific (37–17°S, 103–76°W)-ENSO correlation (denoted as R_3) among the CMIP5 models (Figure 10d). These results support our previous argument that in addition to SSTAs in the southeast Pacific, SSTAs in the southwest Pacific may also be important in initiating ENSO, and the southwest Pacific may serve as an important conduit through which the SPQ affects ENSO.

The ensemble-mean differences in the seasonally averaged SST and surface wind anomalies between strongly positive and negative SPQ events and between strongly positive and negative SPMM events are also evaluated in the CMIP5 preindustrial simulations (Figure 11). The CMIP5 model results show clearly that the western equatorial Pacific westerly anomalies associated with the SPQ tend to be stronger from MAM to SON (September–November) than those associated with the SPMM. As a result, the warming in the central-eastern equatorial Pacific associated with the SPQ has an amplitude greater than that associated with the SPMM from austral spring to winter. These results from the CMIP5 models are very similar to those from observations, supporting the idea that the SPQ could exert a larger influence than the SPMM on ENSO.

6. Summary and Discussion

This study has focused on a detailed investigation of the differences between the SPQ and SPMM. Our results show that SPQ and SPMM have differences in their spatial patterns, temporal variations, and climate impacts. The SPQ exhibits a zonal SSTA pattern with four centers over the extratropical South Pacific, whereas the SPMM exhibits a northeast-southwest-tilted meridional SSTA structure in the South Pacific.

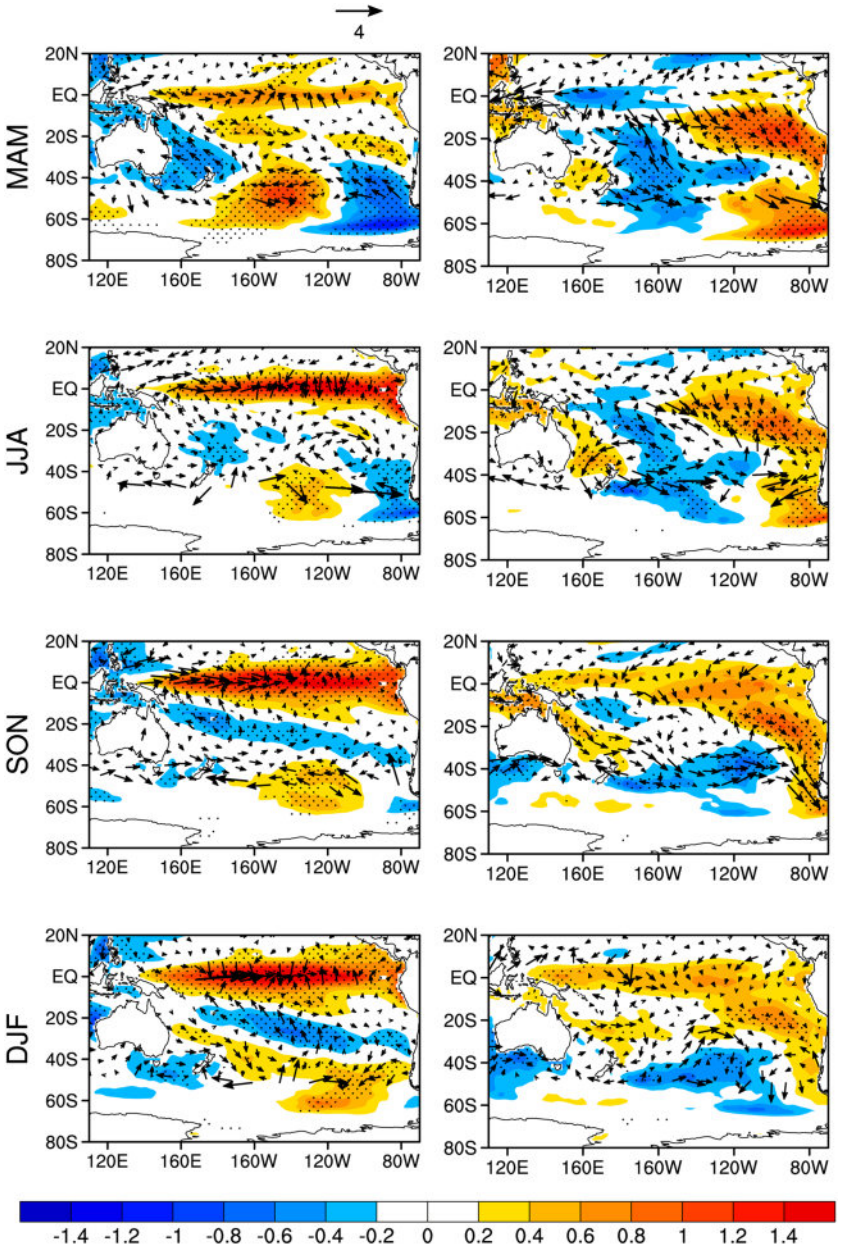

Figure 11. Ensemble-mean composite differences of the 3-month averaged SST (°C; shaded) and surface wind (m s^{-1}; vectors) anomalies between strongly positive and negative SPQ cases (left panel) and between strongly positive and negative SPMM cases (right panel) from preindustrial simulations of 23 CMIP5 models for several lead times (MAM, JJA, SON, and DJF). Positive (red) and negative (blue) SST anomalies, significant at the 95% confidence level, are shaded. Only surface wind vectors significant at the 95% confidence level are shown.

The SPMM has large SSTAs mainly confined to the subtropical southeast Pacific, and SSTAs associated with the SPMM have smaller amplitudes than those associated with the SPQ over the southwest Pacific as well as over high latitudes of the South Pacific. The atmospheric forcing of the SPMM is related to a northeast-southwest-oriented SLPA dipole with a nodal point near 50°S, while the atmospheric forcing of the SPQ is related to a zonal wavenumber-3 SLPA structure in the extratropical South Pacific. The SPQ owns its own temporal variability independent of the SPMM, and strong SPQ events do not always occur simultaneously with strong SPMM events.

Our findings are generally consistent with those from previous studies that both the SPQ and SPMM modes could affect the subsequent development of ENSO events (Ding, Li, & Tseng, 2015; Min et al., 2017; You &

Furtato, 2018; Zhang, Clement, & Di Nezio, 2014). However, our results emphasize that the SPQ, as a basin-scale SST mode over the South Pacific, is more closely linked than the SPMM to ENSO. Therefore, compared with the SPMM, the SPQ may act as an improved precursor signal for ENSO events. The SPQ exerts stronger effects than the SPMM on ENSO, possibly because the SPQ includes an additional role of SSTAs in the southwest Pacific as well as in the high latitudes of the South Pacific. In contrast to SSTAs in the southeast Pacific that may exert effects on ENSO primarily through the thermodynamics, SSTAs in the southwest Pacific may contribute more directly to the oceanic Kelvin wave activity (as a response to westerly wind anomalies) in the western tropical Pacific, which could trigger the Bjerknes dynamical feedback and hence the initiation of ENSO events. However, it should be pointed out that although compared with the SPMM, the SPQ may act as an improved precursor signal for ENSO events, there is no guarantee that the SPQ is a good predictor of ENSO. For example, Larson and Kirtman (2014) reported that the NPMM is a very reliable precursor to ENSO but is not a good predictor due to a large number of false alarms. Further analyses are needed to apply the statistical or dynamical models to test the performance of the SPQ/SPMM precursors as predictors of ENSO.

The current work complements a growing body of literature on the role of the South Pacific SST modes in tropical Pacific climate variability and has implications for understanding the respective role of SSTAs over different regions of the South Pacific in triggering ENSO. Our results suggest that including the role of SSTAs from the southwest Pacific and high-latitude South Pacific might improve ENSO predictability. Further study is needed to investigate the role of the SPQ in enhancing the predictability of ENSO. Note also that while our results highlight the importance of the SPQ to the initiation of El Niño events, we cannot neglect the unique role of the SPMM in tropical Pacific climate variability. At the beginning of 2014, a super El Niño was predicted to occur in the subsequent boreal winter. However, the 2014 event suffered an abrupt termination, and the eventual outcome was a weak El Niño event. Several studies argued that the sudden termination of the 2014 El Niño event was largely attributed to negative SSTAs in the southeast Pacific (Min et al., 2015; Zhu et al., 2016). Further analyses are needed to explore the contribution of negative SSTAs in the southeast Pacific in opposing El Niño development.

Acknowledgments
This work was jointly supported by the National Natural Science Foundation of China (Grant 41790474) and the 973 Project of China (2016YFA0601801). The atmospheric reanalysis dataset was obtained from NCEP/NCAR (available online at https://www.esrl.noaa.gov/psd/data/gridded/data.ncep.reanalysis.html). The HadISST dataset was obtained from the U.K. Met Office Hadley Centre (available online at http://www.metoffice.gov.uk/hadobs/hadsst3/). The subsurface ocean temperature dataset was available online at ftp://ds1.iap.ac.cn/ftp/cheng/CZ16_v3_IAP_Temperature_gridded_1month_netcdf/. The Coupled Model Intercomparison Project Phase 5 (CMIP5) model data can be found at https://cmip.llnl.gov/cmip5/data_portal.html.

References

Bjerknes, J. (1969). Atmospheric teleconnections from the equatorial Pacific. *Monthly Weather Review*, *97*, 163–172.
Chang, P., Zhang, L., Saravanan, R., Vimont, D. J., Chiang, J. C. H., Ji, L., et al. (2007). Pacific meridional mode and El Niño–Southern Oscillation. *Geophysical Research Letters*, *34*, L16608. https://doi.org/10.1029/2007GL030302
Cheng, L., Trenberth, K., Fasullo, J., Boyer, T., Abraham, J., & Zhu, J. (2017). Improved estimates of ocean heat content from 1960 to 2015. *Science Advances*, *3*(3), e1601545. https://doi.org/10.1126/sciadv.1601545
Chiang, J., & Vimont, D. J. (2004). Analogous Pacific and Atlantic meridional modes of tropical atmosphere–ocean variability. *Journal of Climate*, *17*, 4143–4158.
Ding, R. Q., Li, J. P., & Tseng, Y. H. (2015). The impact of South Pacific extratropical forcing on ENSO and comparisons with the North Pacific. *Climate Dynamics*, *44*, 2017–2034.
Ding, R. Q., Li, J. P., Tseng, Y. H., Sun, C., & Guo, Y. P. (2015). The Victoria mode in the North Pacific linking extratropical sea level pressure variations to ENSO. *Journal of Geophysical: Research*, *120*, 27–45. https://doi.org/10.1002/2014JD022221
Holbrook, N. J., & Bindoff, N. L. (1997). Interannual and decadal temperature variability in the southwest Pacific Ocean between 1955 and 1988. *Journal of Climate*, *10*, 1035–1049.
Kalnay, E., Kanamitsu, M., Kistler, R., Collins, W., Deaven, D., Gandin, L., et al. (1996). The NCEP–NCAR 40-year reanalysis project. *Bulletin of the American Meteorological Society*, *77*, 437–471.
Larson, S. M., & Kirtman, B. P. (2013). The Pacific meridional mode as a trigger for ENSO in a high-resolution coupled model. *Geophysical Research Letters*, *40*, 3189–3194.
Larson, S. M., & Kirtman, B. P. (2014). The Pacific meridional mode as an ENSO precursor and predictor in the North American multi-model ensemble. *Journal of Climate*, *27*, 7018–7032.
Larson, S. M., Pegion, K. V., & Kirtman, B. P. (2018). The South Pacific meridional mode as a thermally driven source of ENSO amplitude modulation and uncertainty. *Journal of Climate*, *31*, 5127–5145.
Lin, C. Y., Yu, J. Y., & Hsu, H. H. (2015). CMIP5 model simulations of the Pacific meridional mode and its connection to the two types of ENSO. *International Journal of Climatology*, *35*, 2352–2358.
Matei, D., Keenlyside, N., Latif, M., & Jungclaus, J. (2008). Subtropical forcing of tropical Pacific climate and decadal ENSO modulation. *Journal of Climate*, *21*, 4691–4709.
Min, Q., Su, J., Zhang, R., & Rong, X. (2015). What hindered the El Niño pattern in 2014? *Geophysical Research Letters*, *42*, 6762–6770. https://doi.org/10.1002/2015GL064899
Min, Q. Y., Su, J. Z., & Zhang, R. H. (2017). Impact of the South and North Pacific meridional modes on the El Niño–Southern Oscillation: Observational analysis and comparison. *Journal of Climate*, *30*, 1705–1720.
North, G. R., Bell, T. L., Cahalan, R. F., & Moeng, F. J. (1982). Sampling errors in the estimation of empirical orthogonal function. *Monthly Weather Review*, *110*, 699–706.
Qin, J. H., Ding, R. Q., Wu, Z. W., Li, J., & Zhao, S. (2017). Relationships between the extratropical ENSO precursor and leading modes of atmospheric variability in the Southern Hemisphere. *Advances in Atmospheric Sciences*, *34*, 360–370.

Rayner, N. A., Brohan, P., Parker, D. E., Folland, C. K., Kennedy, J. J., Vanicek, M., et al. (2006). Improved analyses of changes and uncertainties in sea surface temperature measured in situ since the mid-nineteenth century: The HadSST2 dataset. *Journal of Climate*, *19*, 446–469.

Rogers, J. C. (1981). The North Pacific Oscillation. *Journal of Climatology*, *1*, 39–57.

Taylor, K. E., Stouffer, R. J., & Meehl, G. A. (2012). An overview of CMIP5 and the experiment design. *Bulletin of the American Meteorological Society*, *93*, 485–498.

Toniazzo, T. (2010). Climate variability in the south-eastern tropical Pacific and its relation with ENSO: A GCM study. *Climate Dynamics*, *34*, 1093–1114.

Vimont, D. J., Battisti, D. S., & Hirst, A. C. (2003). The seasonal footprinting mechanism in the CSIRO general circulation models. *Journal of Climate*, *16*, 2653–2667.

Vimont, D. J., Wallace, J. M., & Battisti, D. S. (2003). The seasonal footprinting mechanism in the Pacific: Implications for ENSO. *Journal of Climate*, *16*, 2668–2675.

Xie, S. P., & Philander, S. G. H. (1994). A coupled ocean–atmosphere model of relevance to the ITCZ in the eastern Pacific. *Tellus*, *46A*, 340–350.

You, Y. J., & Furtato, J. C. (2018). The South Pacific meridional mode and its role in tropical Pacific climate variability. *Journal of Climate*, *31*, 10,141–10,163.

Zhang, H. H., Clement, A., & Di Nezio, P. (2014). The South Pacific meridional mode: A mechanism for ENSO-like variability. *Journal of Climate*, *27*, 769–783.

Zhang, H. H., Deser, C., Clement, A., & Tomas, R. (2014). Equatorial signatures of the Pacific meridional modes: Dependence on mean climate state. *Geophysical Research Letters*, *41*, 2. https://doi.org/10.1002/2013GL058842

Zhang, L., Chang, P., & Ji, L. (2009). Linking the Pacific meridional mode to ENSO: Coupled model analysis. *Journal of Climate*, *22*, 3488–3505.

Zheng, J., & Wang, F. (2017). On the formation of the South Pacific quadrupole mode. *Theoretical and Applied Climatology*, *130*, 331–344.

Zhu, J. S., Kumar, A., Huang, B. H., Balmaseda, M. A., Hu, Z.-Z., Marx, L., & Kinter, J. L. III (2016). The role of off-equatorial surface temperature anomalies in the 2014 El Niño prediction. *Scientific Reports*, *6*, 19677. https://doi.org/10.1038/srep19677